Chapter 16

Quasi-Geostrophic Dynamics

ABSTRACT
At timescales longer than about a day, geophysical flows are ordinarily in a nearly geostrophic state, and it is advantageous to capitalize on this property to obtain a simplified dynamical formalism. Here, we derive the traditional quasi-geostrophic dynamics and present some applications in both linear and nonlinear regimes. The central component of quasi-geostrophic models, namely advection of vorticity, requires particular attention in numerical models, for which the Arakawa Jacobian is presented.

16.1 SIMPLIFYING ASSUMPTION

Rotation effects become important when the Rossby number is on the order of unity or less (Sections 1.5 and 4.5). The smaller is the Rossby number, the stronger is the rotation effect, and the larger is the Coriolis force compared with the inertial force. In fact, the majority of atmospheric and oceanic motions are characterized by Rossby numbers sufficiently below unity ($Ro \sim 0.2$ down to 0.01), enabling us to state that, in first approximation, the Coriolis force is dominant. This leads to geostrophic equilibrium (Section 7.1) with a balance struck between the Coriolis force and the pressure-gradient force. In Chapter 7, a theory was developed for perfectly geostrophic flows, whereas in Chapter 9 some near-geostrophic, small-amplitude waves were investigated. In each case, the analysis was restricted to homogeneous flows. Here, we reconsider near-geostrophic motions but in the case of continuously stratified fluids and nonlinear dynamics. Much of the material presented can be traced to the seminal article by Charney[1] (1948), which laid the foundation of quasi-geostrophic dynamics.

Geostrophic balance is a linear and diagnostic relationship; there is no product of variables and no time derivative. The resulting mathematical advantages explain why near-geostrophic dynamics are used routinely: The underlying assumption of near-geostrophy may not always be strictly valid, but the formalism is much simpler than otherwise.

[1] See biographical sketch at the end of the chapter.

Introduction to Geophysical Fluid Dynamics, Volume 101, ISSN 0074-6142, DOI: 10.1016/B978-0-12-088759-0.00016-X

Mathematically, a state of near-geostrophic balance occurs when the terms representing relative acceleration, nonlinear advection, and friction are all negligible in the horizontal momentum equations. This requires (Section 4.5) that the temporal Rossby number,

$$Ro_T = \frac{1}{\Omega T}, \tag{16.1}$$

the Rossby number,

$$Ro = \frac{U}{\Omega L}, \tag{16.2}$$

and the Ekman number,

$$Ek = \frac{\nu_E}{\Omega H^2}, \tag{16.3}$$

all be small simultaneously. In these expressions, Ω is the angular rotation rate of the earth (or planet or star under consideration), T is the timescale of the motion (i.e., the time span over which the flow field evolves substantially), U is a typical horizontal velocity in the flow, L is the horizontal length over which the flow extends or exhibits variations, ν_E is the eddy vertical viscosity, and H is the vertical extent of the flow.

The smallness of the Ekman number (Section 4.5) indicates that vertical friction is negligible, except perhaps in thin layers on the edges of the fluid domain (Chapter 8). If we exclude small-amplitude waves that can travel much faster than fluid particles in the flow, the temporal Rossby number (16.1) is not greater than the Rossby number (16.2). (For a discussion of this argument, the reader is referred to Section 9.1.) By elimination, it remains to require that the Rossby number (16.2) be small. This can be justified in one of the two ways: Either velocities are relatively weak (small U) or the flow pattern is laterally extensive (large L). The common approach, and the one that leads to the simplest formulation, is to consider the first possibility; the resulting formalism bears the name of *quasi-geostrophic dynamics*. We ought to keep in mind, however, that some atmospheric and oceanic motions could be nearly geostrophic for the other reason, that is, large velocities on a large scale (Cushman-Roisin, 1986). Such motions are called frontal geostrophic and would be improperly represented by quasi-geostrophic dynamics.

16.2 GOVERNING EQUATION

To set the stage for the development of quasi-geostrophic equations, it is most convenient to begin with the restriction that vertical displacements of density surfaces be small (Fig. 16.1). In the (x, y, z) coordinate system, we write

$$\rho = \bar{\rho}(z) + \rho'(x, y, z, t) \quad \text{with} \quad |\rho'| \ll |\bar{\rho}|. \tag{16.4}$$

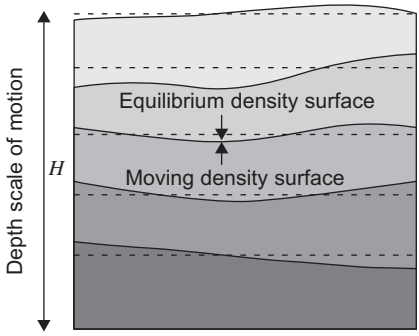

FIGURE 16.1 A rotating stratified fluid undergoing weak motions, which can be described by quasi-geostrophic dynamics.

Because the density surfaces are nearly horizontal, there is no real advantage to be gained by using the density-coordinate system, and we follow the tradition here by formulating the quasi-geostrophic dynamics in the (x, y, z) Cartesian coordinate system.

The density profile $\bar{\rho}(z)$, independent of time and horizontally uniform, forms the basic stratification. Alone, it creates a state of rest in hydrostatic equilibrium. We shall assume that such stratification has somehow been established, and that it is maintained in time against the homogenizing action of vertical diffusion. The quasi-geostrophic formalism does not consider the origin and maintenance of this stratification but only the behavior of motions that weakly perturb it.

The following mathematical developments are purposely heuristic, with emphasis on the exploitation of the main idea rather than on a systematic approach. The reader interested in a rigorous derivation of quasi-geostrophic dynamics based on a regular perturbation analysis is referred to Chapter 6 of the book by Pedlosky (1987).

The governing equations of Section 4.4 with $\rho = \bar{\rho}(z) + \rho'(x, y, z, t)$ and, similarly, $p = \bar{p}(z) + p'(x, y, z, t)$ are on the beta plane and, for simplicity, in the absence of friction and diffusion:

$$\frac{\mathrm{d}u}{\mathrm{d}t} - f_0 v - \beta_0 y v = -\frac{1}{\rho_0}\frac{\partial p'}{\partial x} \tag{16.5a}$$

$$\frac{\mathrm{d}v}{\mathrm{d}t} + f_0 u + \beta_0 y u = -\frac{1}{\rho_0}\frac{\partial p'}{\partial y} \tag{16.5b}$$

$$0 = -\frac{\partial p'}{\partial z} - \rho' g \tag{16.5c}$$

$$\frac{\partial u}{\partial x} + \frac{\partial v}{\partial y} + \frac{\partial w}{\partial z} = 0 \tag{16.5d}$$

$$\frac{\partial \rho'}{\partial t} + u\frac{\partial \rho'}{\partial x} + v\frac{\partial \rho'}{\partial y} + w\frac{\mathrm{d}\bar{\rho}}{\mathrm{d}z} = 0, \tag{16.5e}$$

where the advective operator is

$$\frac{\mathrm{d}}{\mathrm{d}t} = \frac{\partial}{\partial t} + u\frac{\partial}{\partial x} + v\frac{\partial}{\partial y} + w\frac{\partial}{\partial z}. \tag{16.6}$$

The basic assumption that $|\rho'|$ is much less than $|\bar{\rho}|$ has been implemented in the density Eq. (16.5e) by dropping the term $w\partial\rho'/\partial z$. In writing that equation, we have also neglected density diffusion (the right-hand side of the equation) in agreement with our premise that the basic vertical stratification persists. Finally, because the basic stratification is in hydrostatic equilibrium with the pressure at rest, the corresponding terms cancel out, and only the perturbed pressure p', that due to motion, appears in the equations.

If the density perturbations ρ' are small, so are the pressure disturbances p', and by virtue of the horizontal momentum equations, the horizontal velocities are weak. While the Coriolis terms are small, the nonlinear advective terms, which involve products of velocities, are even smaller. For expediency, we shall use the phrase *very small* for these and all other terms smaller than the small terms. Thus, the ratio of advective to Coriolis terms, the Rossby number, is small. Let us assume now and verify *a posteriori* that the timescale is long compared with the inertial period $(2\pi/f_0)$, so the local-acceleration terms are, too, very small. Finally, to guarantee that the beta-plane approximation holds, we further require $|\beta_0 y| \ll f_0$. Having made all these assumptions, we take pleasure in noting that the dominant terms in the momentum equations are, as expected, those of the geostrophic equilibrium:

$$-f_0 v = -\frac{1}{\rho_0}\frac{\partial p'}{\partial x} \tag{16.7a}$$

$$+f_0 u = -\frac{1}{\rho_0}\frac{\partial p'}{\partial y}. \tag{16.7b}$$

As noted in Chapter 7, this geostrophic state is singular, for it leads to a zero horizontal divergence $(\partial u/\partial x + \partial v/\partial y = 0)$, which usually (e.g., over a flat bottom) implies the absence of any vertical velocity. In the case of a stratified fluid, this in turn implies no lifting and lowering of density surfaces, and thus no pressure disturbances and no variations in time.

To explore dynamics beyond such a simple state of affairs, we consider that the velocity includes a small ageostrophic (not geostrophic) correction and write

$$u = u_g + u_a, \quad v = v_g + v_a, \tag{16.8}$$

in which the first terms represent the geostrophic component, defined as

$$u_g = -\frac{1}{f_0\rho_0}\frac{\partial p'}{\partial y} \tag{16.9a}$$

$$v_g = +\frac{1}{f_0\rho_0}\frac{\partial p'}{\partial x}, \tag{16.9b}$$

and (u_a, v_a) are the ageostrophic corrections.

In the smaller time-derivatives, advection and beta terms of Eqs. (16.5a) and (16.5b), we replace the velocity by its geostrophic approximation (16.7), while we care to retain both geostrophic and ageostrophic components in the larger Coriolis terms. Because it is small compared with horizontal advection, itself already a small correction term compared with the Coriolis term, vertical advection is neglected, and we obtain the following:

$$-\frac{1}{\rho_0 f_0}\frac{\partial^2 p'}{\partial y \partial t}-\frac{1}{\rho_0^2 f_0^2}J\left(p',\frac{\partial p'}{\partial y}\right)-f_0 v-\frac{\beta_0}{\rho_0 f_0}y\frac{\partial p'}{\partial x}=-\frac{1}{\rho_0}\frac{\partial p'}{\partial x} \tag{16.10a}$$

$$+\frac{1}{\rho_0 f_0}\frac{\partial^2 p'}{\partial x \partial t}+\frac{1}{\rho_0^2 f_0^2}J\left(p',\frac{\partial p'}{\partial x}\right)+f_0 u-\frac{\beta_0}{\rho_0 f_0}y\frac{\partial p'}{\partial y}=-\frac{1}{\rho_0}\frac{\partial p'}{\partial y} \tag{16.10b}$$

The symbol $J(\cdot,\cdot)$ stands for the Jacobian operator, defined as $J(a,b)=(\partial a/\partial x)(\partial b/\partial y)-(\partial a/\partial y)(\partial b/\partial x)$.

From these equations, more accurate expressions for u and v can be readily extracted:

$$\begin{aligned} u=u_g+u_a=&-\frac{1}{\rho_0 f_0}\frac{\partial p'}{\partial y}-\frac{1}{\rho_0 f_0^2}\frac{\partial^2 p'}{\partial t \partial x}\\ &-\frac{1}{\rho_0^2 f_0^3}J\left(p',\frac{\partial p'}{\partial x}\right)+\frac{\beta_0}{\rho_0 f_0^2}y\frac{\partial p'}{\partial y} \end{aligned} \tag{16.11a}$$

$$\begin{aligned} v=v_g+v_a=&+\frac{1}{\rho_0 f_0}\frac{\partial p'}{\partial x}-\frac{1}{\rho_0 f_0^2}\frac{\partial^2 p'}{\partial t \partial y}\\ &-\frac{1}{\rho_0^2 f_0^3}J\left(p',\frac{\partial p'}{\partial y}\right)-\frac{\beta_0}{\rho_0 f_0^2}y\frac{\partial p'}{\partial x} \end{aligned} \tag{16.11b}$$

which, unlike Eq. (16.7), contain both the geostrophic flow and a first series of ageostrophic corrections. This improved estimate of the flow field has a nonzero divergence, which is small because it is caused solely by the weak velocity departures from the otherwise nondivergent geostrophic flow.

Upon substitution of these expressions in continuity equation (16.5d), we obtain

$$\frac{\partial w}{\partial z}=\frac{1}{\rho_0 f_0^2}\left[\frac{\partial}{\partial t}\nabla^2 p'+\frac{1}{\rho_0 f_0}J(p',\nabla^2 p')+\beta_0\frac{\partial p'}{\partial x}\right], \tag{16.12}$$

where $\nabla^2=\partial^2/\partial x^2+\partial^2/\partial y^2$ is the two-dimensional Laplacian operator. We note that the right-hand arises only because of ageostrophic components. Thus, the vertical velocity is on the order of ageostrophic terms, and this justifies *a posteriori* our dropping of the w-terms from advection.

We now turn our attention to the density-conservation equation (16.5e). The first term is very small because ρ' is small, and the timescale is long. Likewise,

the last term is very small because, as we concluded before, the vertical velocity arises from the ageostrophic corrections to the already weak horizontal velocity. The middle terms involve the density perturbation, which is small, and the horizontal velocities, which are also small. There is thus no need, in this equation, for the corrections brought by Eq. (16.11), and the geostrophic expressions (16.7) suffice, leaving

$$\frac{\partial \rho'}{\partial t} + \frac{1}{\rho_0 f_0} J(p', \rho') - \frac{\rho_0 N^2}{g} w = 0, \tag{16.13}$$

in which the stratification frequency, $N^2(z) = -(g/\rho_0)\mathrm{d}\bar{\rho}/\mathrm{d}z$, has been introduced. Dividing this last equation by N^2/g, taking its z-derivative, and using the hydrostatic balance (16.5c) to eliminate density, we obtain

$$\frac{\partial}{\partial t}\left[\frac{\partial}{\partial z}\left(\frac{1}{N^2}\,\frac{\partial p'}{\partial z}\right)\right] + \frac{1}{\rho_0 f_0} J\left[p', \frac{\partial}{\partial z}\left(\frac{1}{N^2}\,\frac{\partial p'}{\partial z}\right)\right] + \rho_0 \frac{\partial w}{\partial z} = 0. \tag{16.14}$$

Equations (16.12) and (16.14) form a two-by-two system for the perturbation pressure p' and vertical stretching $\partial w/\partial z$. Elimination of $\partial w/\partial z$ between the two yields a single equation for p':

$$\frac{\partial}{\partial t}\left[\nabla^2 p' + \frac{\partial}{\partial z}\left(\frac{f_0^2}{N^2}\,\frac{\partial p'}{\partial z}\right)\right] + \frac{1}{\rho_0 f_0} J\left[p', \nabla^2 p' + \frac{\partial}{\partial z}\left(\frac{f_0^2}{N^2}\,\frac{\partial p'}{\partial z}\right)\right] + \beta_0 \frac{\partial p'}{\partial x} = 0. \tag{16.15}$$

This is the quasi-geostrophic equation for nonlinear motions in a continuously stratified fluid on a beta plane. Usually, this equation is recast as an equation for the potential vorticity, and the pressure field is transformed into a streamfunction ψ through $p' = \rho_0 f_0 \psi$. The result is

$$\frac{\partial q}{\partial t} + J(\psi, q) = 0, \tag{16.16}$$

where q is the potential vorticity:

$$q = \nabla^2 \psi + \frac{\partial}{\partial z}\left(\frac{f_0^2}{N^2}\,\frac{\partial \psi}{\partial z}\right) + \beta_0 y. \tag{16.17}$$

Once the solution is obtained for q and ψ, the original variables can be recovered from Eqs. (16.7a), (16.7b), and (16.13):

$$u_g = -\frac{\partial \psi}{\partial y} \tag{16.18a}$$

$$v_g = +\frac{\partial \psi}{\partial x} \tag{16.18b}$$

$$u_a = -\frac{1}{f_0}\frac{\partial^2 \psi}{\partial t \partial x} - \frac{1}{f_0} J\left(\psi, \frac{\partial \psi}{\partial x}\right) + \frac{\beta_0}{f_0} y \frac{\partial \psi}{\partial y} \tag{16.18c}$$

$$v_a = -\frac{1}{f_0}\frac{\partial^2 \psi}{\partial t \partial y} - \frac{1}{f_0} J\left(\psi, \frac{\partial \psi}{\partial y}\right) - \frac{\beta_0}{f_0} y \frac{\partial \psi}{\partial x} \tag{16.18d}$$

$$w = -\frac{f_0}{N^2}\left[\frac{\partial^2 \psi}{\partial t \partial z} + J\left(\psi, \frac{\partial \psi}{\partial z}\right)\right] \tag{16.18e}$$

$$p' = \rho_0 f_0 \psi \tag{16.18f}$$

$$\rho' = -\frac{\rho_0 f_0}{g}\frac{\partial \psi}{\partial z}. \tag{16.18g}$$

If turbulent dissipation is retained in the formalism, the equation governing the evolution of potential vorticity becomes complicated, but an approximation suitable for most numerical applications is as follows:

$$\frac{\partial q}{\partial t} + J(\psi, q) = \frac{\partial}{\partial x}\left(\mathcal{A}\frac{\partial q}{\partial x}\right) + \frac{\partial}{\partial y}\left(\mathcal{A}\frac{\partial q}{\partial y}\right) + \frac{\partial}{\partial z}\left(\nu_E \frac{\partial q}{\partial z}\right), \tag{16.19}$$

where q remains defined by Eq. (16.17).

16.3 LENGTH AND TIMESCALE

Expression (16.17) indicates that q is a form of potential vorticity. Indeed, the last term represents the planetary contribution to the vorticity, whereas the first term, $\nabla^2 \psi = \partial v/\partial x - \partial u/\partial y$, is the relative vorticity. The middle term can be traced to the layer-thickness variations in the denominator of the classical definition of potential vorticity [e.g., Eq. (12.21)]. Indeed, in view of Eq. (16.18g), this term measures vertical variations of ρ', directly related to thickness changes between density surfaces. It is thus a linear version of vertical stretching (see Analytical Problem 16.7). Although expression (16.17) for q does not have the same dimension as potential vorticity defined in Eq. (12.21), we shall follow common practice here and not coin another name but call it potential vorticity.

It is most interesting to compare the first two terms of the potential-vorticity expression, namely, relative vorticity and vertical stretching. With L and U as

the horizontal length and velocity scales, respectively, the streamfunction ψ scales like LU by virtue of Eqs. (16.18a) and (16.18b). If H is the vertical length scale, not necessarily the fluid depth, the magnitudes of those contributions to potential vorticity are as follows:

$$\text{Relative vorticity} \sim \frac{U}{L}, \quad \text{Vertical stretching} \sim \frac{f_0^2 UL}{N^2 H^2}. \tag{16.20}$$

The ratio of the former to the latter is

$$\frac{\text{Relative vorticity}}{\text{Vertical stretching}} \sim \frac{N^2 H^2}{f_0^2 L^2} = Bu, \tag{16.21}$$

which is the Burger number defined in Section 11.6. For weak stratification or long length scale (i.e., small Burger number, $NH \ll f_0 L$), vertical stretching dominates, and the motion is akin to that of homogeneous rotating flows in nearly geostrophic balance (Chapter 7), where topographic variations are capable of exerting great influence. For large Burger numbers ($NH \gg f_0 L$), that is, strong stratification or short length scales, relative vorticity dominates, stratification reduces coupling in the vertical, and every level tends to behave in a two-dimensional fashion, stirred by its own vorticity pattern, independently of what occurs above and below.

The richest behavior occurs when the stratification and length scale match to make the Burger number of order unity, which occurs when

$$L = \frac{NH}{f_0}. \tag{16.22}$$

As noted in Section 12.2, this particular length scale is the internal radius of deformation. To show this, let us introduce a nominal density difference $\Delta\rho$, typical of the density vertical variations of the ambient stratification. Thus, $|\mathrm{d}\bar{\rho}/\mathrm{d}z| \sim \Delta\rho/H$ and $N^2 \sim g\Delta\rho/\rho_0 H$. Defining a reduced gravity as $g' = g\Delta\rho/\rho_0$, which is typically much less than the full gravity g, we obtain

$$N \sim \sqrt{\frac{g'}{H}}. \tag{16.23}$$

Definition (16.22) yields

$$L \sim \frac{\sqrt{g'H}}{f_0}. \tag{16.24}$$

Comparing this expression with definition (9.12) for the radius of deformation in homogeneous rotating fluids, we note the replacement of the full gravitational acceleration by a much smaller, reduced acceleration and conclude that motions in stratified fluids tend to take place on shorter scales than dynamically similar motions in homogeneous fluids.

Before concluding this section, it is noteworthy to return to the discussion of the timescale. Very early in the derivation, an assumption was made to restrict the attention to slowly evolving motions, namely, motions with timescale T much longer than the inertial timescale $1/f_0$ (i.e., $T \gg \Omega^{-1}$). This relegated the terms $\partial u/\partial t$ and $\partial v/\partial t$ to the rank of small perturbations to the dominant geostrophic balance. Now, having completed our analysis, we ought to check for consistency.

The timescale of quasi-geostrophic motions can be most easily determined by inspection of the governing equation in its potential-vorticity form. The balance of Eq. (16.16) requires that the two terms on its left-hand side be of the same order:

$$\frac{Q}{T} \sim \frac{UL}{L}\frac{Q}{L},$$

where Q is the scale of potential vorticity, regardless of whether it is dominated by relative vorticity ($Q \sim U/L$) or vertical stretching ($Q \sim f_0^2 UL/N^2H^2$), and LU is the streamfunction scale. The preceding statement yields

$$T \sim \frac{L}{U}, \tag{16.25}$$

in other words, the timescale is advective. The quasi-geostrophic structure evolves on a time T comparable to the time taken by a particle to cover the length scale L at the nominal speed U. For example, a vortex flow (such as an atmospheric cyclone) evolves significantly while particles complete one revolution.

Because the quasi-geostrophic formalism is rooted in the smallness of the Rossby number ($Ro = U/\Omega L \ll 1$), it follows directly that the timescale must be long compared with the rotation period:

$$T \gg \frac{1}{\Omega}, \tag{16.26}$$

in agreement with our premise. Note, however, that a lack of contradiction is proof only of consistency in the formalism. It implies that slowly evolving, quasi-geostrophic motions can exist, but the existence of other, non-quasi-geostrophic motions are certainly not precluded. Among the latter, we can distinguish nearly geostrophic motions of other types (Cushman-Roisin, 1986; Cushman-Roisin, Sutyrin & Tang, 1992; Phillips, 1963) and, of course, completely ageostrophic motions (see examples in Chapters 13 and 15). Whereas ageostrophic flows typically evolve on the inertial timescale ($T \sim \Omega^{-1}$), geostrophic motions of type other than quasi-geostrophic usually evolve on much longer timescales ($T \gg L/U \gg \Omega^{-1}$).

16.4 ENERGETICS

Because the quasi-geostrophic formalism is frequently used, it is worth investigating the approximate energy budget that is associated with it. Multiplying the governing equation (16.16) by the streamfunction ψ and integrating over the entire three-dimensional domain, we obtain, after several integrations by parts:

$$\frac{\mathrm{d}}{\mathrm{d}t}\iiint \frac{1}{2}\rho_0|\nabla\psi|^2\mathrm{d}x\,\mathrm{d}y\,\mathrm{d}z + \frac{\mathrm{d}}{\mathrm{d}t}\iiint \frac{1}{2}\,\rho_0\frac{f_0^2}{N^2}\left(\frac{\partial\psi}{\partial z}\right)^2 \mathrm{d}x\,\mathrm{d}y\,\mathrm{d}z = 0. \tag{16.27}$$

The boundary terms have all been set to zero by assuming rigid bottom and top surfaces, and, in the horizontal, any combination of periodicity, vertical wall, or decay at large distances.

Equation (16.27) can be interpreted as a mechanical-energy budget: The sum of kinetic and potential energies is conserved over time. That the first integral corresponds to kinetic energy is evident once the velocity components have been expressed in terms of the streamfunction ($u^2+v^2=\psi_y^2+\psi_x^2=|\nabla\psi|^2$). By default, this leaves the second integral to play the role of potential energy, which is not as evident. Basic physical principles would indeed suggest the following definition for potential energy:

$$PE = \iiint \rho g z\,\mathrm{d}x\,\mathrm{d}y\,\mathrm{d}z, \tag{16.28}$$

which by virtue of Eq. (16.18g) would yield a linear, rather than a quadratic, expression in ψ.

The discrepancy is resolved by defining the *available potential energy*, a concept first advanced by Margules (1903) and developed by Lorenz (1955). Because the fluid occupies a fixed volume, the rising of fluid in some locations must be accompanied by a descent of fluid elsewhere; therefore, any potential-energy gain somewhere is necessarily compensated, at least partially, by a potential-energy drop elsewhere. What matters then is not the total potential energy of the fluid but only how much could be converted from the instantaneous, perturbed density distribution. We define the available potential energy, *APE*, as the difference between the existing potential energy, as just defined, and the potential energy that the fluid would have if the basic stratification were unperturbed.

The situation is best illustrated in the case of a two-layer stratification (Fig. 16.2): A lighter fluid of density ρ_1 floats atop of a denser fluid of density ρ_2. In the presence of motion, the interface is at level a above the resting height H_2 of the lower layer. Because of volume conservation, the integral of a over the horizontal domain vanishes identically. The potential energy associated

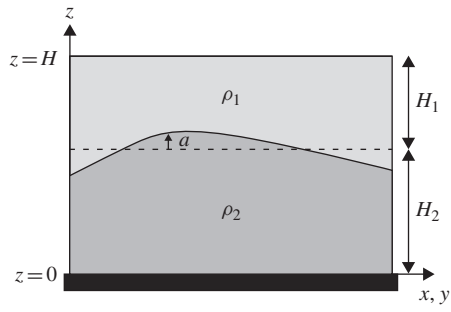

FIGURE 16.2 A two-layer stratification, for the illustration of the concept of available potential energy.

with the perturbed state is

$$\begin{aligned} PE(a) &= \iint \left[\int_0^{H_2+a} \rho_2 g z \, \mathrm{d}z + \int_{H_2+a}^{H} \rho_1 g z \, \mathrm{d}z \right] \mathrm{d}x\mathrm{d}y \\ &= \iint \left[\frac{1}{2}\rho_1 g H^2 + \frac{1}{2}\Delta\rho g H_2^2 \right] \mathrm{d}x\mathrm{d}y \\ &+ \iint \Delta\rho H_2 a \, \mathrm{d}x\mathrm{d}y + \iint \frac{1}{2}\Delta\rho g a^2 \, \mathrm{d}x\mathrm{d}y, \end{aligned}$$

where H is the total height, and $\Delta\rho = \rho_2 - \rho_1$ is the density difference. The first term represents the potential energy in the unperturbed state, whereas the second term vanishes because a has a zero mean. This leaves the third term as the available potential energy:

$$\begin{aligned} APE &= PE(a) - PE(a=0) \\ &= \iint \frac{1}{2}\Delta\rho g a^2 \, \mathrm{d}x\mathrm{d}y. \end{aligned} \tag{16.29}$$

Introducing the stratification frequency $N^2 = -(g/\rho_0)\mathrm{d}\bar{\rho}/\mathrm{d}z = g\Delta\rho/\rho_0 H$ and generalizing to three dimensions, we obtain

$$APE = \iiint \frac{1}{2}\rho_0 N^2 a^2 \mathrm{d}x\,\mathrm{d}y\,\mathrm{d}z. \tag{16.30}$$

In continuous stratification, the vertical displacement a of a fluid parcel is directly related to the density perturbation because the density anomaly at one point is created by moving to that point a particle that originates from a different vertical level:

$$\begin{aligned} \rho'(x,y,z,t) &= \bar{\rho}[z - a(x,y,z,t)] - \bar{\rho}(z) \\ &\simeq -a\frac{\mathrm{d}\bar{\rho}}{\mathrm{d}z} = \frac{\rho_0 N^2}{g}a. \end{aligned} \tag{16.31}$$

This Taylor expansion is justified by the underlying assumption of weak vertical displacements. Combining Eqs. (16.30) and (16.31) and expressing the density perturbation in terms of the streamfunction by Eq. (16.18g), we obtain

$$APE = \iiint \frac{1}{2}\rho_0 \frac{f_0^2}{N^2}\left(\frac{\partial \psi}{\partial z}\right)^2 \mathrm{d}x\,\mathrm{d}y\,\mathrm{d}z, \tag{16.32}$$

which is the integral that arises in the energy budget, (16.27).

The time rate of change of the available potential energy can be expressed as

$$\frac{\mathrm{d}}{\mathrm{d}t}APE = g\iiint \rho' w\,\mathrm{d}x\,\mathrm{d}y\,\mathrm{d}z, \tag{16.33}$$

as can be verified by substitution of Eqs. (16.18e) and (16.18g) into Eq. (16.33) and an integration by parts of the Jacobian term. This shows that potential energy increases when heavy fluid parcels rise (ρ' and w both positive) and light parcels sink (ρ' and w both negative).

As a final note, we observe that a scale analysis provides the ratio of kinetic energy, *KE*, to available potential energy *APE*:

$$\frac{KE}{APE} \sim \frac{N^2H^2}{L^2f^2} \sim Bu, \tag{16.34}$$

which gives another interpretation to the Burger number: It compares kinetic to potential energy.

16.5 PLANETARY WAVES IN A STRATIFIED FLUID

In Chapter 9, it was noted that inertia-gravity waves are superinertial ($\omega \geq f$) and that Kelvin waves require a fundamentally ageostrophic balance in one of the two horizontal directions [see Eq. (9.4b) with $u = 0$]. Therefore, the quasi-geostrophic formalism cannot describe these two types of waves. It can, however, describe the slow waves and, in particular, the planetary waves that exist on the beta plane.

It is instructive to explore the three-dimensional behavior of planetary (Rossby) waves in a continuously stratified fluid. The theory proceeds from the linearization of the quasi-geostrophic equation and, for mathematical simplicity only, the assumptions of a constant stratification frequency and no dissipation. Equations (16.16) and (16.17) then yield

$$\frac{\partial}{\partial t}\left(\nabla^2\psi + \frac{f_0^2}{N^2}\frac{\partial^2\psi}{\partial z^2}\right) + \beta_0\frac{\partial \psi}{\partial x} = 0. \tag{16.35}$$

We seek a wave solution of the form $\psi(x, y, z, t) = \phi(z)\cos(k_x x + k_y y - \omega t)$, with horizontal wavenumbers k_x and k_y, frequency ω, and amplitude $\phi(z)$. The

vertical structure of the amplitude is governed by

$$\frac{\mathrm{d}^2\phi}{\mathrm{d}z^2} - \frac{N^2}{f_0^2}\left(k_x^2 + k_y^2 + \frac{\beta_0 k_x}{\omega}\right)\phi = 0, \tag{16.36}$$

which results from the substitution of the wave solution into Eq. (16.35). To solve this equation, boundary conditions are necessary in the vertical. For these, let us assume that our fluid is bounded below by a horizontal surface and above by a free surface. In the atmosphere, this situation would correspond to the troposphere above a flat terrain or sea and below the tropopause.

At the bottom (say, $z = 0$), the vertical velocity vanishes, and the linearized form of Eq. (16.18e) implies $\partial^2\psi/\partial z\partial t = 0$, or

$$\frac{\mathrm{d}\phi}{\mathrm{d}z} = 0 \quad \text{at} \quad z = 0. \tag{16.37}$$

At the free surface [say, $z = h(x, y, t)$], the pressure is uniform. Because the total pressure consists of the hydrostatic pressures due to the reference density ρ_0 (eliminated when the Boussinesq approximation was made; see Section 3.7) and to the basic stratification $\bar{\rho}(z)$, together with the perturbation pressure caused by the wave, we write:

$$P_0 - \rho_0 g z + g\int_z^h \bar{\rho}(z')\,\mathrm{d}z' + p'(x, y, h, t) = \text{constant}, \tag{16.38}$$

at the free surface $z = h$. Because particles on the free surface remain on the free surface at all times (there is no inflow/outflow), we also state

$$w = \frac{\partial h}{\partial t} + u\frac{\partial h}{\partial x} + v\frac{\partial h}{\partial y} \quad \text{at} \quad z = h. \tag{16.39}$$

The preceding two statements are then linearized. Writing $h = H + \eta$, where the free-surface displacement $\eta(x, y, t)$ is small to justify linear wave motions, we expand the variables p' and w in Taylor fashion from the mean surface level $z = H$ and systematically drop all terms involving products of variables of the wave field. The two requirements then reduce to

$$-\rho_0 g\eta + p' = 0 \quad \text{and} \quad w = \frac{\partial \eta}{\partial t} \quad \text{at} \quad z = H. \tag{16.40}$$

Elimination of η yields $\partial p'/\partial t = \rho_0 g w$ and, in terms of the streamfunction,

$$\frac{\partial}{\partial t}\left(\frac{\partial \psi}{\partial z} + \frac{N^2}{g}\psi\right) = 0 \quad \text{at} \quad z = H \tag{16.41}$$

or, finally, in terms of the wave amplitude,

$$\frac{\mathrm{d}\phi}{\mathrm{d}z}+\frac{N^2}{g}\phi=0 \quad \text{at} \quad z=H. \tag{16.42}$$

Together, Eq. (16.36) and its two boundary conditions, Eqs. (16.37) and (16.42), define an eigenvalue problem, which admits solutions of the form

$$\phi(z)=A\cos k_z z \tag{16.43}$$

already satisfying boundary condition (16.37). Substitution of this solution into Eq. (16.36) yields the dispersion relation linking the wave frequency ω to the wavenumber components, k_x, k_y, and k_z:

$$\omega=-\frac{\beta_0 k_x}{k_x^2+k_y^2+k_z^2 f_0^2/N^2}, \tag{16.44}$$

whereas substitution into boundary condition (16.42) imposes a condition on the wavenumber k_z:

$$\tan k_z H=\frac{N^2 H}{g}\frac{1}{k_z H}. \tag{16.45}$$

As Fig. 16.3 demonstrates graphically, there is an infinite number of discrete solutions. Because negative values of k_z lead to solutions identical to those with positive k_z values [see Eqs. (16.43) and (16.44)], it is necessary to consider only the latter set of values ($k_z>0$).

A return to the definition $N^2=-(g/\rho_0)\mathrm{d}\bar{\rho}/\mathrm{d}z$ reveals that the ratio N^2H/g, appearing on the right-hand side of Eq. (16.45), is equal to $\Delta\rho/\rho_0$, where $\Delta\rho$ is the density difference between top and bottom of the basic stratification $\bar{\rho}(z)$. The factor N^2H/g is thus very small, implying that the first solution of Eq. (16.45) falls very near the origin (Fig. 16.3). There, $\tan k_z H$ can be approximated to $k_z H$, yielding

$$k_z H = \frac{NH}{\sqrt{gH}}. \tag{16.46}$$

The fraction on the right is the ratio of the internal gravity wave speed to the surface gravity wave speed, which is small. Note also that this mode disappears in the limit $g\to\infty$, which we would have obtained if we had imposed a rigid lid at the top of the domain.

Because $k_z H$ is small, the corresponding wave is nearly uniform in the vertical. Its dispersion relation, obtained from the substitution of the preceding value of k_z into Eq. (16.44),

$$\omega=-\frac{\beta_0 k_x}{k_x^2+k_y^2+f_0^2/gH}, \tag{16.47}$$

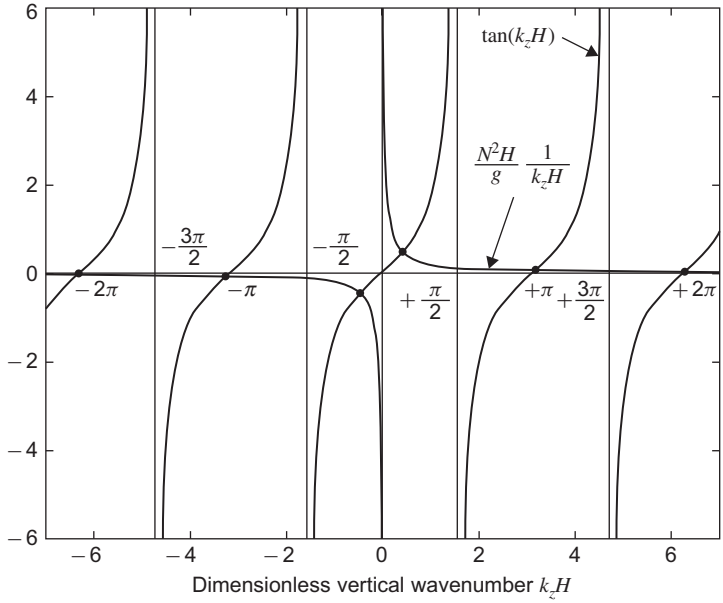

FIGURE 16.3 Graphical solution of Eq. (16.45). Every crossing of curves yields an acceptable value for the vertical wavenumber k_z. The pair of values nearest to the origin corresponds to a solution fundamentally different from all others.

is independent of the stratification frequency N and identical to the dispersion relation obtained for planetary waves in homogeneous fluids [see Eq. (9.27)]. Because it is almost uniform in the vertical, we conclude that this wave is the barotropic component of the set.

The remaining solutions for k_z can also be determined to the same degree of approximation. Because N^2H/g is small, the finite solutions of Eq. (16.45) fall very near the zeros of $\tan k_z H$ (Fig. 16.3) and are thus given approximately by

$$k_{z_n} = n\frac{\pi}{H}, \quad n = 1,\ 2,\ 3,\ \ldots \tag{16.48}$$

Unlike the barotropic wave, the waves with these wavenumbers exhibit substantial variations in the vertical and can be called *baroclinic*. Their dispersion relation,

$$\omega_n = -\frac{\beta_0 k_x}{k_x^2 + k_y^2 + (n\pi f_0/NH)^2}, \tag{16.49}$$

is morphologically identical to Eq. (16.47), implying that they, too, are planetary waves. In summary, the presence of stratification permits the existence of an infinite, discrete set of planetary waves, one barotropic and all other baroclinic.

Comparing the dispersion relations Eqs. (16.47) and (16.49) of the barotropic and baroclinic waves, we note the replacement in the denominator of the ratio f_0^2/gH by a multiple of $(\pi f_0/NH)^2$, which is much larger, since—again—N^2H/g is very small. Physically, the barotropic component is influenced by the large, external radius of deformation $\sqrt{gH}/f_0$ [see Eq. (9.12)], whereas the baroclinic waves feel the much shorter, internal radius of deformation NH/f_0 [see Eq. (16.22)].

In the atmosphere, there is not always a great disparity between the two radii of deformation. Take, for example, a midlatitude region (such as 45°N, where $f_0 = 1.03 \times 10^{-4}\,\mathrm{s}^{-1}$), a tropospheric height $H = 10\,\mathrm{km}$, and a stratification frequency $N = 0.01\,\mathrm{s}^{-1}$. This yields $\sqrt{gH}/f_0 = 3050\,\mathrm{km}$ and $NH/f_0 = 972\,\mathrm{km}$. (The ratio N^2H/g is then 0.102, which is not very small.) In contrast, the difference between the two radii of deformation is much more pronounced in the ocean. Take, for example, $H = 3\,\mathrm{km}$ and $N = 2 \times 10^{-3}\,\mathrm{s}^{-1}$, which yield $\sqrt{gH}/f_0 = 1670\,\mathrm{km}$ and $NH/f_0 = 58\,\mathrm{km}$.

In any event, all planetary waves exhibit a zonal phase speed. For the baroclinic members of the family, it is

$$c_n = \frac{\omega_n}{k_x} = -\frac{\beta_0}{k_x^2 + k_y^2 + (n\pi f_0/NH)^2}. \tag{16.50}$$

Because this quantity is always negative, the direction can only be westward.[2] Moreover, the westward speed is confined to the interval

$$-\beta_0 R_n^2 < c_n < 0, \tag{16.51}$$

with the lower bound approached by the longest wave ($k_x^2 + k_y^2 \to \infty$). The lengths R_n, defined as

$$R_n = \frac{1}{n}\frac{NH}{\pi f_0}, \quad n = 1,\ 2,\ 3,\ \ldots \tag{16.52}$$

are identified as internal radii of deformation, one for each baroclinic mode. The greater the value of n, the greater the value of k_{zn}, the more reversals the wave exhibits in the vertical, and the more restricted is its zonal propagation. Therefore, the waves most active in transmitting information and carrying energy from east to west (or from west to east, if the group velocity is positive) are the barotropic and the first baroclinic component. Indeed, observations reveal that these two modes alone carry generally 80–90% of the energy in the ocean.

Let us now turn our attention to the spatial structure of a baroclinic planetary wave. For simplicity, we take the first mode ($n = 1$), which corresponds to a

[2] The meridional phase speed, ω_n/k_y, may be either positive or negative, depending on the sign of k_y.

wave with one reversal of the flow in the vertical, and we set k_y to zero to focus on the zonal profile of the wave. The streamfunction, pressure, and density distributions are as follows:

$$\psi = A\cos k_z z \cos(k_x x - \omega t) \tag{16.53a}$$

$$p' = \rho_0 f_0 \psi = \rho_0 f_0 A \cos k_z z \cos(k_x x - \omega t) \tag{16.53b}$$

$$\rho' = -\frac{\rho_0 f_0}{g}\frac{\partial \psi}{\partial z} = +\frac{\rho_0 f_0 k_z}{g} A \sin k_z z \cos(k_x x - \omega t). \tag{16.53c}$$

The geostrophic velocity component is

$$u_g = -\frac{\partial \psi}{\partial y} = 0 \tag{16.54a}$$

$$v_g = +\frac{\partial \psi}{\partial x} = -k_x A \cos k_z z \sin(k_x x - \omega t), \tag{16.54b}$$

and we immediately recognize that it cannot be responsible for the wave because it has no associated vertical velocity needed to displace density surfaces and allow energy conversion between kinetic and potential energy. Hence, the essence of the dynamics resides in the ageostrophic velocity component,

$$\begin{aligned} u_a &= -\frac{1}{f_0}\frac{\partial^2 \psi}{\partial t \partial x} \\ &= -\frac{k_x \omega}{f_0} A \cos k_z z \cos(k_x x - \omega t) \end{aligned} \tag{16.55a}$$

$$\begin{aligned} v_a &= -\frac{\beta_0}{f_0} y \frac{\partial \psi}{\partial x} \\ &= +\frac{\beta_0 k_x}{f_0} y A \cos k_z z \sin(k_x x - \omega t) \end{aligned} \tag{16.55b}$$

$$\begin{aligned} w &= -\frac{f_0}{N^2}\frac{\partial^2 \psi}{\partial t \partial z} \\ &= +\frac{f_0 \omega k_z}{N^2} A \sin k_z z \sin(k_x x - \omega t). \end{aligned} \tag{16.55c}$$

We leave it as an exercise to the reader to verify that the three-dimensional divergence of the ageostrophic motion is zero as it should. The corresponding wave structure is displayed in Fig. 16.4 and can be interpreted as follows.

At the bottom, vertical displacements are prohibited, and there is no density anomaly. At the surface, vertical displacements would only be important if it were the barotropic (external) mode, but this is a baroclinic (internal) mode, and vertical displacements are negligible at the top. In the interior, however, vertical displacements are significant, with one maximum at midlevel for the lowest baroclinic mode (depicted here). Where the middle density surface rises,

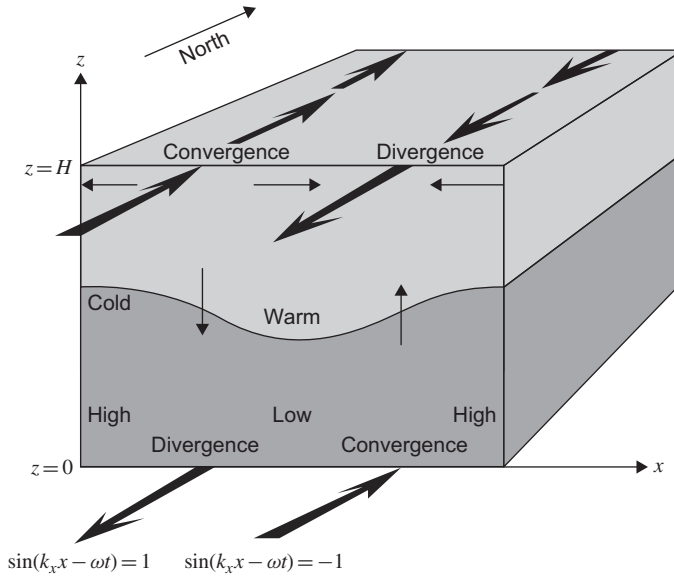

FIGURE 16.4 Structure of a baroclinic planetary wave. In constructing this diagram, we have taken $f_0 > 0$, $k_x > 0$, $k_y = 0$, and $k_z = \pi/H$, which yield $\omega < 0$ and a wave structure with a single reversal in the vertical.

heavier (colder) fluid from below is found, forming a cold anomaly. Similarly, a warm anomaly accompanies a subsidence, half a wavelength away. Because colder fluid is heavier and warmer fluid is lighter, the bottom pressure is higher under cold anomalies and lower under warm anomalies. At the lowest order of approximation, the resulting zonal pressure gradient drives an alternating geostrophic meridional flow v_g given by Eq. (16.54b). In the northern hemisphere (as depicted in Fig. 16.4), the bottom velocity has the higher pressure on its right and, therefore, assumes a southward direction east of the high pressures and a northward direction east of the low pressures. Because of the baroclinic nature of the wave, there is a reversal in the vertical, and the velocities near the top are counter to those below (Fig. 16.4).

On the beta plane, the variation in the Coriolis parameter causes this meridional flow to be convergent or divergent. In the northern hemisphere, the northward increase of f implies, under a uniform pressure gradient, a decreasing velocity and thus convergence of northward flow and divergence of southward flow. The resulting convergence–divergence pattern calls for transverse ageostrophic velocities, either zonal or vertical or both. According to Fig. 16.4, based on Eqs. (16.55c) and (16.55a), both transverse components come into play, each partially relieving the convergence–divergence of the

meridional flow. The relative importance of vertical to horizontal convergence is

$$\frac{k_z W}{k_x U} = \frac{f_0^2 k_z^2}{N^2 k_x^2}, \tag{16.56}$$

and we recover the inverse of the Burger number based on the length scales of the wave.

The ensuing vertical velocities at midlevel cause subsidence below a convergence and above a divergence, feeding the excess of the upper flow into the deficit of that underneath, and create uplifting half a wavelength away, where the situation is vertically reversed. Subsidence generates a warm anomaly, while uplifting generates a cold anomaly. As we can see in Fig. 16.4, this takes place a quarter of a wavelength to the west of the existing anomalies, thus inducing a westward shift of the wave pattern overtime. The result is a wave pattern steadily translating to the west.

16.6 SOME NONLINEAR EFFECTS

In its original form, the quasi-geostrophic equation (16.16) is quadratic in the streamfunction. An assumption of weak amplitudes was, therefore, necessary to explore the linear wave regime, and it is proper to ask now what role nonlinearities could play. For evident reasons, no general solution of the nonlinear equation is available. Nonlinearities cause interactions among the existing waves, generating harmonics and spreading the energy over a wide spectrum of scales. According to numerical simulations (McWilliams, 1989; Rhines, 1977), the result is a complicated unsteady state of motion, which has been termed *geostrophic turbulence*.

Although this topic will be more fully developed in a later chapter (Section 18.3), it is worth mentioning here the natural tendency of geostrophic turbulence to form coherent structures (McWilliams, 1984, 1989). These take the form of distinct and robust vortices that can be clearly identified and traced for periods of time long compared with their turn-around times. Figure 18.17 provides an example. The vortices contain a disproportionate amount of the energy available, being therefore highly nonlinear and leaving a relatively weak and linear wavefield in the intermediate space. In other words, a mature state of geostrophic turbulence displays a dichotomous pattern of nonlinear, localized vortices and linear, nonlocalized waves.

To explore nonlinear effects, let us seek a localized, vortex-type solution of finite amplitude. To simplify the analysis, we make the following assumptions of inviscid fluid and uniform stratification ($N =$ constant). Furthermore, expecting a possible zonal drift reminiscent of planetary waves, we seek solutions that are

steadily translating in the x-direction. Thus, we state

$$\frac{\partial q}{\partial t} + J(\psi, q) = 0 \tag{16.57}$$

$$q = \nabla^2\psi + \frac{f_0^2}{N^2}\frac{\partial^2\psi}{\partial z^2} + \beta_0 y, \tag{16.58}$$

in which $\psi = \psi(x - ct, y, z)$ is a function vanishing at large distances.

Because the variables x and t occur only in the combination $x - ct$, the time derivative can be assimilated to an x-derivative ($\partial/\partial t = -c\partial/\partial x$) and the equation becomes

$$J(\psi + cy, q) = 0,$$

which admits the general solution

$$q = \nabla^2\psi + \frac{f_0^2}{N^2}\frac{\partial^2\psi}{\partial z^2} + \beta_0 y = F(\psi + cy). \tag{16.59}$$

The function F is, at this stage, an arbitrary function of its variable, $\psi + cy$. Because the vortex is required to be localized, the streamfunction must vanish at large distances, including large zonal distances at finite values of the meridional coordinate y. From Eq. (16.59), this implies

$$\beta_0 y = F(cy),$$

and the function F is linear: $F(\alpha) = (\beta_0/c)\alpha$. Naturally, the function F may be multivalued, taking values along contours of $\psi + cy$ not connected to infinity (and, therefore, closed onto themselves within the confines of the vortex) that are different from the values along other, open contours of $\psi + cy$. In other words, the same $\psi + cy$ on two different contours could correspond to two distinct values of F.

Mindful of this possibility but restricting our attention for now to the region extending to infinity, where F is linear, we have from Eq. (16.59)

$$\nabla^2\psi + \frac{f_0^2}{N^2}\frac{\partial^2\psi}{\partial z^2} = \frac{\beta_0}{c}\psi. \tag{16.60}$$

Now, assuming the existence of rigid surfaces at the top and bottom, we impose $\partial\psi/\partial z = 0$ at $z = 0$ and H, restricting the number of vertical modes. The gravest baroclinic mode has the structure $\psi = a(r, \theta)\cos(\pi z/H)$, where (r, θ) are the polar coordinates associated with the Cartesian coordinates $(x - ct, y)$. The horizontal structure of the solution is prescribed by the amplitude $a(r, \theta)$, which must satisfy

$$\frac{\partial^2 a}{\partial r^2} + \frac{1}{r}\frac{\partial a}{\partial r} - \frac{1}{r^2}\frac{\partial^2 a}{\partial \theta^2} - \left(\frac{1}{R^2} + \frac{\beta_0}{c}\right)a = 0, \tag{16.61}$$

by virtue of Eq. (16.60). Here,

$$R = \frac{NH}{\pi f_0}, \tag{16.62}$$

is the internal radius of deformation. (The factor π is introduced here for convenience.) Such an equation admits solutions consisting of sinusoidal functions in the azimuthal direction and Bessel functions in the radial direction.

Because the potential energy is proportional to the integrated square of the vertical displacements, a localized vortex structure of finite energy requires a streamfunction field (proportional to a) that decays at large distances faster than $1/r$. This requirement excludes the Bessel functions of the first kind, which decay only as $r^{-1/2}$ and leaves us with the modified Bessel functions, which decay exponentially:

$$a(r,\theta) = \sum_{m=0}^{\infty} (A_m \cos m\theta + B_m \sin m\theta) K_m(kr), \tag{16.63}$$

where the factor k defined by

$$k^2 = \frac{1}{R^2} + \frac{\beta_0}{c} \tag{16.64}$$

must be real. The condition that k be real implies, from Eq. (16.64) that the drift speed c of the vortex must be either less than $-\beta_0 R^2$ or greater than zero. In other words, c must lie outside of the range of linear planetary wave speeds [see Eq. (16.51)]. Because k enters the solution in multiplication with the radial distance r, its inverse, $1/k$, can be considered as the width of the vortex:

$$L = \frac{1}{k} = \frac{R}{\sqrt{1 + \beta_0 R^2/c}}. \tag{16.65}$$

The faster the propagation (either eastward or westward), the closer L is to the deformation radius R. Eastward-propagating vortices ($c > 0$) are smaller than R, whereas westward-propagating ones ($c < 0$) are wider.

The Bessel functions K_m are singular at the origin, and solution (16.63) fails near the vortex center. The situation is remedied by requiring that in the vicinity of $r = 0$, the function F assumes another form than that used previously, changing the character of the solution there. Here, we shall not consider this solution, called the *modon*, and instead refer the interested reader to Flierl, Larichev, McWilliams and Reznik (1980).

Let us now consider disturbances on a zonal jet, such as the meanders of the atmospheric Jet Stream. Waves and finite-amplitude perturbations propagate zonally at a net speed that is their own drift speed plus the jet average velocity. They thus move away from their region of origin, such as a mountain range, by traveling either upstream or downstream, unless their net speed is about zero. In this last case, when the disturbance's own speed c is equal and opposite to the

average jet velocity U, the disturbance is stationary and can persist for a much longer time. Typically, the zonal jet flows eastward (Jet Stream in the atmosphere, Gulf Stream in the ocean, and prevailing winds on Jupiter at the latitude of the Great Red Spot), and so we take U positive. The mathematical requirement is $c = -U$ (westward), and two cases arise: Either U is smaller than $\beta_0 R^2$ or it is not. For U less than $\beta_0 R^2$, c falls in the range of planetary waves, and the disturbance is a train of planetary waves, giving the jet a meandering character. By virtue of dispersion relation (16.50), applied to the gravest vertical mode ($n = 1$) and to the zero meridional wavenumber ($m = 0$), the zonal wavelength is

$$\lambda = \frac{2\pi}{k_x} = 2\pi R \sqrt{\frac{U}{\beta_0 R^2 - U}}. \tag{16.66}$$

If the jet velocity varies downstream, the wavelength adjusts locally, increasing with U. However, if U exceeds $\beta_0 R^2$, finite-amplitude, isolated disturbances are possible, and the jet may be strongly distorted. The preceding theory suggests the following length scale

$$L = \frac{1}{k} = R \sqrt{\frac{U}{U - \beta_0 R^2}}. \tag{16.67}$$

16.7 QUASI-GEOSTROPHIC OCEAN MODELING

Quasi-geostrophic models were at the core of the first weather-forecast systems (see biographies at the end of Chapter 5 and of the present chapter), and the reason for their success was their highly simplified mathematics and numerics while capturing the dynamics essential to weather forecasting. Because of limited computing power, the first few models were two-dimensional. Here, we illustrate the core numerical properties of these two-dimensional models because they are representative of the numerics used in the subsequent three-dimensional models.

In two dimensions, in the absence of friction and turbulence, the equation governing quasi-geostrophic dynamics reduces to

$$\frac{\partial q}{\partial t} + J(\psi, q) = 0 \tag{16.68}$$

with the potential vorticity q defined as

$$q = \nabla^2 \psi + \beta_0 y. \tag{16.69}$$

It is clear from Eq. (16.68) that the Jacobian J operator plays a central role in the mathematics. This Jacobian can be expressed mathematically in

several different ways:

$$J(\psi,q) = \frac{\partial\psi}{\partial x}\frac{\partial q}{\partial y} - \frac{\partial\psi}{\partial y}\frac{\partial q}{\partial x} \tag{16.70a}$$

$$= \frac{\partial}{\partial x}\left(\psi\frac{\partial q}{\partial y}\right) - \frac{\partial}{\partial y}\left(\psi\frac{\partial q}{\partial x}\right) \tag{16.70b}$$

$$= \frac{\partial}{\partial y}\left(q\frac{\partial\psi}{\partial x}\right) - \frac{\partial}{\partial x}\left(q\frac{\partial\psi}{\partial y}\right) \tag{16.70c}$$

so that we can readily write the corresponding finite-difference forms, all of second order (see Fig. 16.5 for notation):

$$J^{++} = \frac{(\tilde{\psi}_4-\tilde{\psi}_8)(\tilde{q}_6-\tilde{q}_2)-(\tilde{\psi}_6-\tilde{\psi}_2)(\tilde{q}_4-\tilde{q}_8)}{4\Delta x\Delta y} \tag{16.71a}$$

$$J^{+\times} = \frac{\left[\tilde{\psi}_4(\tilde{q}_5-\tilde{q}_3)-\tilde{\psi}_8(\tilde{q}_7-\tilde{q}_1)\right]-\left[\tilde{\psi}_6(\tilde{q}_5-\tilde{q}_7)-\tilde{\psi}_2(\tilde{q}_3-\tilde{q}_1)\right]}{4\Delta x\Delta y} \tag{16.71b}$$

$$J^{\times+} = \frac{\left[\tilde{q}_6(\tilde{\psi}_5-\tilde{\psi}_7)-\tilde{q}_2(\tilde{\psi}_3-\tilde{\psi}_1)\right]-\left[\tilde{q}_4(\tilde{\psi}_5-\tilde{\psi}_3)-\tilde{q}_8(\tilde{\psi}_7-\tilde{\psi}_1)\right]}{4\Delta x\Delta y} \tag{16.71c}$$

With a multiplicity of discretizations at our disposal, we may wonder which leads to the best model. Because all are second order, we have to invoke other properties than truncation error to decide on the optimal discretization, such as conservation laws. We can, for example, identify the following integral constraints over a 2D domain of surface $\mathcal{S}$ within a close impermeable boundary

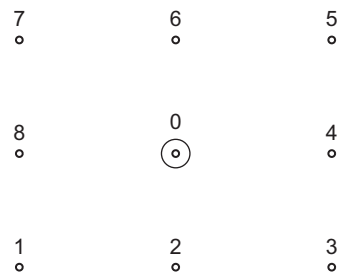

FIGURE 16.5 Grid notation for Jacobian $J(\psi,q)$ around the central point labeled 0. The discretization J^{++} (16.71a) uses ψ and q at side points 2, 4, 6, and 8, and $J^{+\times}$ (16.71b) takes ψ values at side points 2, 4, 6, 8 and q values at corner points 1, 3, 5, and 7, while $J^{\times+}$ switches the values of ψ and q.

(uniform ψ along the boundary) or with periodic boundaries:

$$\int_{\mathcal{S}} J(\psi, q)\, \mathrm{d}\mathcal{S} = 0, \tag{16.72}$$

$$\int_{\mathcal{S}} qJ(\psi, q)\, \mathrm{d}\mathcal{S} = 0, \tag{16.73}$$

$$\int_{\mathcal{S}} \psi J(\psi, q)\, \mathrm{d}\mathcal{S} = 0. \tag{16.74}$$

Expression (16.74) can be related to the evolution of kinetic energy. In addition, we have an antisymmetry property:

$$J(\psi, q) = -J(q, \psi). \tag{16.75}$$

Numerical discretization generally does not ensure conservation of the corresponding integral properties in the discrete solution. Akio Arakawa (see biography at the end of Chapter 9) had the brilliant idea of combining different versions of the discretized Jacobian in order to preserve those properties in the discrete formulation. The combination

$$J = (1-\alpha-\beta)J^{++} + \alpha J^{+\times} + \beta J^{\times+} \tag{16.76}$$

for any value of α and β leads to a consistent discretization. We should, therefore, try to assign those values of α and β that ensure as many simultaneous conservation properties as possible.

Integral (16.74) in its discrete form sums up individual terms involving products $\psi_{i,j}J_{i,j}$ or, with the shorter notation of Fig. 16.5, terms such as

$$\Delta x \Delta y\, \psi_0 J_0. \tag{16.77}$$

For the Jacobian discretized according to Eq. (16.71a), this involves

$$4\Delta x \Delta y\, \tilde{\psi}_0 J_0^{++} = \tilde{\psi}_0\tilde{\psi}_4(\tilde{q}_6 - \tilde{q}_2) + \cdots \tag{16.78}$$

The sum (integral) over the domain includes the contribution $\psi_4 J_4$, in which we find similar terms with the opposite sign:

$$4\Delta x \Delta y\, \tilde{\psi}_4 J_4^{++} = -\tilde{\psi}_0\tilde{\psi}_4(\tilde{q}_5 - \tilde{q}_3) + \cdots \tag{16.79}$$

but the terms do not cancel each other because of the differing q values. However, if we look at the alternative discretization $J^{+\times}$, we do find the terms that do cause cancellation:

$$4\Delta x \Delta y\, \tilde{\psi}_0 J_0^{+\times} = \tilde{\psi}_0\tilde{\psi}_4(\tilde{q}_5 - \tilde{q}_3) + \cdots \tag{16.80}$$

and

$$4\Delta x\Delta y\,\tilde{\psi}_4 J_4^{+\times} \;=\; -\tilde{\psi}_4\tilde{\psi}_0(\tilde{q}_6-\tilde{q}_2)+\cdots \tag{16.81}$$

So, if we add $(J^{++}+J^{+\times})$ and then integrate over the domain, the ψJ products cancel one another out in pairs. The same reasoning applies to other combinations of terms such as those between point 0 and 6. Thus, constraint (16.74) is respected if $(J^{++}+J^{+\times})/2$ is used for the discretization of the Jacobian.

There is better. Because $\psi J^{\times+}$ does not contain the terms $\tilde{\psi}_0\tilde{\psi}_4$ and $\tilde{\psi}_0\tilde{\psi}_6$ but contains terms with the product $\tilde{\psi}_0\tilde{\psi}_5$

$$4\Delta x\Delta y\,\tilde{\psi}_0 J_0^{\times+} \;=\; \tilde{\psi}_0\tilde{\psi}_5(\tilde{q}_6-\tilde{q}_4)+\cdots \tag{16.82}$$

$$4\Delta x\Delta y\,\tilde{\psi}_5 J_5^{\times+} \;=\; \tilde{\psi}_0\tilde{\psi}_5(\tilde{q}_4-\tilde{q}_6)+\cdots \tag{16.83}$$

which cancel each other out, it turns out that we can dilute the sum $(J^{++}+J^{+\times})$ with any amount of $J^{\times+}$ (make $1-\alpha-\beta$ equal to α while keeping β arbitrary).

Similarly, if we take the sum $(J^{++}+J^{\times+})$ or $J^{+\times}$ or combination, the sum of qJ over all grid points of the domain vanishes, respecting constraint (16.73). Thus, Eqs. (16.74) and (16.73) can be simultaneously respected if we take $1-\alpha-\beta=\alpha=\beta$, which calls for $\alpha=\beta=1/3$.

Let us now check on the antisymmetry condition (16.75). It is satisfied with J^{++} and with the sum $(J^{+\times}+J^{\times+})$. Thus, we happily note that our combination $(J^{++}+J^{+\times}+J^{\times+})/3$ already respects it. In conclusion, the values $\alpha=\beta=1/3$ are ideal because they carry Eqs. (16.73)–(16.75) from the continuum representation over to the discretized formulation. This discretization, which is very popular, has become known as the *Arakawa Jacobian*.

The second essential ingredient in the quasi-geostrophic evolution is the relation between q and ψ. Its core term is

$$q \;=\; \frac{\partial^2\psi}{\partial x^2}+\frac{\partial^2\psi}{\partial y^2}, \tag{16.84}$$

which is also the sole remaining term on the f-plane in two-dimensions. Because Eq. (16.68) provides the equation to advance q in time, Eq. (16.84) can be considered as the equation to be solved for ψ once an updated value has been calculated for q. Hence we need to invert a Poisson equation at each time step, a task already encountered in Section 7.8. In the first quasi-geostrophic models, inversion was done by successive over-relaxation, occasionally with a red–black approach on vector computers.

ANALYTICAL PROBLEMS

16.1. Derive the one-layer quasi-geostrophic equation

$$\frac{\partial}{\partial t}\left(\nabla^2\psi - \frac{1}{R^2}\psi\right) + J(\psi, \nabla^2\psi) + \beta_0\frac{\partial\psi}{\partial x} = 0, \tag{16.85}$$

where $R = (gH)^{1/2}/f_0$, from the shallow-water model (7.17) assuming weak surface displacements. How do the waves permitted by these dynamics compare with the planetary waves exposed in Section 16.5?

16.2. Demonstrate the assertion made at the end of Section 16.4 that the time rate of change of available potential energy is proportional to the integral of the product of density perturbation with vertical velocity.

16.3. Elucidate in a rigorous manner the scaling assumptions justifying simultaneously the quasi-geostrophic approximation and the linearization of the equations for the wave analysis. What is the true restriction on vertical displacements?

16.4. Show that the assumption of a rigid upper surface (combined to the assumption of a flat bottom) effectively replaces the external radius of deformation by infinity. Also show that the approximate solutions for the vertical wavenumber k_z in Section 16.5 then become exact.

16.5. Explore topographic waves using the quasi-geostrophic formalism on an f-plane ($\beta_0 = 0$). Begin by formulating the appropriate bottom-boundary condition.

16.6. Establish the so-called *Omega Equation* on the f-plane for a quasi-geostrophic system without friction and with N^2 horizontally uniform. The Omega Equation provides the vertical velocity in a diagnostic form (i.e., without need for time integration). The formulation involves the geostrophic flow (u_g, v_g) associated with the (observed) density field:

$$N^2\frac{\partial^2 w}{\partial x^2} + N^2\frac{\partial^2 w}{\partial y^2} + f^2\frac{\partial^2 w}{\partial z^2} = \frac{\partial Q_x}{\partial x} + \frac{\partial Q_y}{\partial y} \tag{16.86}$$

with

$$Q_x = +2f\left(\frac{\partial u_g}{\partial z}\frac{\partial v_g}{\partial x} + \frac{\partial v_g}{\partial z}\frac{\partial v_g}{\partial y}\right)$$

$$Q_y = -2f\left(\frac{\partial u_g}{\partial y}\frac{\partial v_g}{\partial z} + \frac{\partial u_g}{\partial z}\frac{\partial u_g}{\partial x}\right).$$

16.7. Show that potential vorticity q defined by Eq. (16.17) is a linearization of potential vorticity $\tilde{q}$ defined in Eq. (12.21) in the sense that for constant N^2

$$\tilde{q} = \frac{f_0}{h_0} + \frac{q}{h_0}, \tag{16.87}$$

in which h_0 is the unperturbed thickness of the layer, and the linearization assumes small vertical displacements and weak horizontal velocities. (*Hint*: The unperturbed height is directly related to N^2. For the linearization, express $1/h$ as a function of vertical density gradients.)

16.8. Take the reduced-gravity version of the quasi-geostrophic equation:

$$\frac{\partial q}{\partial t} = J(\psi, q) \quad \text{with} \quad q = \nabla^2\psi - \frac{\psi}{R^2} + \beta_0 y \tag{16.88}$$

and show that the center of mass of a vortex patch propagates westward at a speed $\beta_0 R^2$, where the coordinates of the center of mass $(X(t),Y(t))$ are defined as

$$X = \frac{\iint x\psi \,\mathrm{d}x\mathrm{d}y}{\iint \psi \,\mathrm{d}x\mathrm{d}y}, \quad Y = \frac{\iint y\psi \,\mathrm{d}x\mathrm{d}y}{\iint \psi \,\mathrm{d}x\mathrm{d}y}, \tag{16.89}$$

(*Hint*: Calculate $\mathrm{d}X/\mathrm{d}t$ and $\mathrm{d}Y/\mathrm{d}t$.)

NUMERICAL EXERCISES

16.1. Verify numerical conservation (16.72) by adapting `qgmodel.m` in a closed two-dimensional domain of size L. Compare leapfrog and explicit Euler time discretizations. Initialize with a streamfunction given by

$$\psi = \omega_0 L^2 \sin\left(\frac{\pi x}{L}\right) \sin\left(\frac{\pi y}{L}\right). \tag{16.90}$$

On all four sides, $x = 0$, $x = L$, $y = 0$, and $y = L$, the boundaries are impermeable, and the streamfunction is kept zero. Use $\omega_0 = 10^{-5}\,\mathrm{s}^{-1}$ and $L = 100\,\mathrm{km}$. For simplicity, also use zero vorticity along the perimeter.

16.2. Start with `qgmodelrun.m` and generalize the code to allow dynamics on the two-dimensional beta plane. Also add superviscosity (biharmonic diffusion) as shown in Section 10.6. Redo the simulation of Numerical Exercise 16.1 including the beta term. Take $\beta_0 = 2 \times 10^{-11}\,\mathrm{m}^{-1}\,\mathrm{s}^{-1}$ and $L = 3000\,\mathrm{km}$. Observe the evolution of the streamfunction. (*Hint*: Keep relative vorticity as the dynamic variable and express the beta effect as a forcing term in the governing equation for relative vorticity, e.g., within the Jacobian operator.)

16.3. Simulate the evolution of an eddy on the f-plane. Begin with an eddy centered at the origin with its streamfunction given by

$$\psi = -\omega_0 L^2 (r+1)\mathrm{e}^{-r}, \qquad r = \frac{\sqrt{x^2+y^2}}{L}, \tag{16.91}$$

with $L = 100\,\mathrm{km}$ and $\omega_0 = 10^{-5}\ \mathrm{s}^{-1}$, and then perturb it by multiplying r used in the initial calculation of ψ by $1+\epsilon\cos(2\theta)$, where θ is the azimuthal angle and ϵ a small parameter, for example, ~ 0.03. Perform the calculations in the square domain $[-10L, 10L]\times[-10L, 10L]$ with zero values for ψ along the perimeter.

16.4. Redo Numerical Exercise 16.3 with an initial eddy defined by

$$\omega = \begin{cases} -\omega_0 & \text{for } 0 < r/L < 1/\sqrt{2} \\ +\omega_0 & \text{for } 1/\sqrt{2} \le r/L < 1 \\ 0 & \text{for } 1 \le r/L \end{cases} \tag{16.92}$$

and verify that you obtain the evolution shown in Fig. 16.6.

16.5. Adapt `qgmodel.m` to simulate the instability of the barotropic flow of Section 10.4 or analyze `shearedflow.m`. Initialize with the basic flow perturbed by an unstable wave. Instead of an infinite domain in the y–direction, prescribe zero values for the streamfunction at $y = \pm 10L$. Apply periodic boundary conditions in the x-direction. What boundary conditions do you use for the potential vorticity q? Which problem related to boundary conditions do you encounter if you want to use biharmonic diffusion (Section 10.6)? In any case, take a weak diffusion for

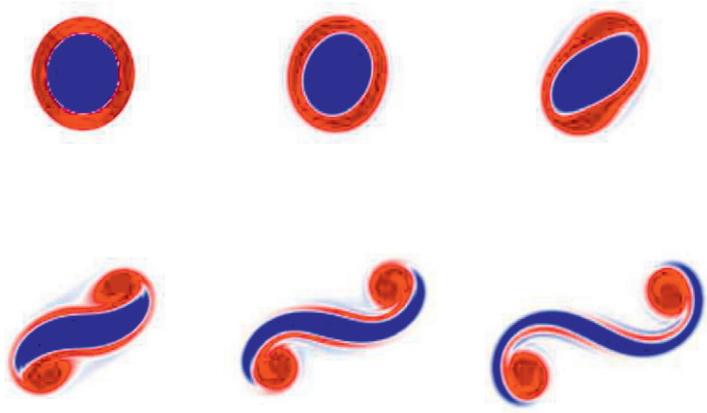

FIGURE 16.6 Evolution of a perturbed vorticity patch within a quasi-geostrophic framework.

the simulations. (*Hint*: Expect to have time for a cup of coffee during the simulation.)

16.6. Implement a more efficient Poisson-equation solver using a conjugate-gradient approach (see Section 7.8) by using MATLAB™ routine `pcg`, and redo Numerical Exercise 16.5. Search the World Wide Web for a multi-grid version of the Poisson equation solver to further reduce calculation times if necessary.

16.7. Adapt the over-relaxation parameter to decrease the computation time of simulations in Numerical Exercise 16.5. Then simulate the schematized atmospheric jet stream of Analytical Problem 10.4, with a long wave-like perturbation. In a second experiment, reduce the intensity of the jet stream by a factor 4. In a third experiment, keep the lower velocity but disable the beta term. Discuss the stability in the context of the solution to Analytical Problem 10.4.

16.8. Simulate the evolution of the triangular jet of Analytical Problem 10.5, with $L = 50$ km and $U = 1$ m/s. (*Hint*: Perturb the zonal flow by a rather long wave in a sufficiently long domain.)

Jule Gregory Charney
1917–1981

A strong proponent of the idea that intelligent simplifications of a problem are not only necessary to obtain answers but also essential to understand the underlying physics, Jule Charney was a major contributor to dynamic meteorology. As a student, he studied the instabilities of large-scale atmospheric flows and elucidated the mechanism that is now called baroclinic instability (Chapter 17). His thesis appeared in 1947, and the following year, he published an article outlining quasi-geostrophic dynamics (the material of this chapter). He then turned his attention to numerical weather prediction, an activity envisioned by L. F. Richardson some 30 years earlier. The success of the initial weather simulations in the early 1950s is to be credited not only to J. von Neumann's first electronic computer, but also to Charney's judicious choice of simplified dynamics, the quasi-geostrophic equation. Later on, Charney was instrumental in convincing officials worldwide of the significance of numerical weather predictions, while he also gained much deserved recognition for his work on tropical meteorology, topographic instability, geostrophic turbulence, and the Gulf Stream. Charney applied his powerful intuition to systematic scale analysis. Scaling arguments are now a mainstay in geophysical fluid dynamics. (*Photo from archives of the Massachusetts Institute of Technology*)

Allan Richard Robinson
1932–2009

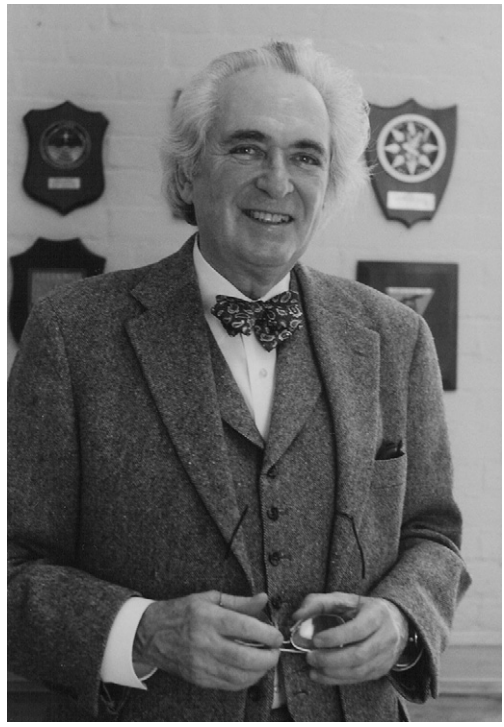

An avowed "phenomenologist," Allan Robinson is counted among the founding fathers of geophysical fluid dynamics because of his seminal contributions on the dynamics of rotating and stratified fluids, boundary-layer flows, continental shelf waves, and the maintenance of the oceanic thermocline. Underlying his accomplishments is the firm belief that "curiosity about nature is the primary driving force and rationalization for research." During the 1970s he chaired and cochaired a series of international programs that established the existence and importance of intermediate-scale eddies in the open ocean, the *internal weather of the sea*. His research led him to formulate numerical models for ocean forecasting and to emphasize the role of ocean physics in regulating biological activity. Robinson has also contributed significantly to the development of techniques for the assimilation of data in ocean-forecasting models. During the 1980s and 1990s, he led a group of international scientists, predominantly from bordering nations, to advance the science of the Mediterranean Sea. Later, he headed a program to synthesize knowledge of the interdisciplinary global coastal ocean. (*A. R. Robinson, Harvard University*)